

Recurrent Self-Supervised Video Denoising with Denser Receptive Field

Zichun Wang*

xiaoding310@gmail.com

Beijing Institute of Technology

Debing Zhang

debingzhangchina@gmail.com

Xiaohongshu Inc

Yulun Zhang*

yulun100@gmail.com

ETH Zürich

Ying Fu[†]

fuying@bit.edu.cn

Beijing Institute of Technology

ABSTRACT

Self-supervised video denoising has seen decent progress through the use of blind spot networks. However, under their blind spot constraints, previous self-supervised video denoising methods suffer from significant information loss and texture destruction in either the whole reference frame or neighbor frames, due to their inadequate consideration of the receptive field. Moreover, the limited number of available neighbor frames in previous methods leads to the discarding of distant temporal information. Nonetheless, simply adopting existing recurrent frameworks does not work, since they easily break the constraints on the receptive field imposed by self-supervision. In this paper, we propose RDRF for self-supervised video denoising, which not only fully exploits both the reference and neighbor frames with a denser receptive field, but also better leverages the temporal information from both local and distant neighbor features. First, towards a comprehensive utilization of information from both reference and neighbor frames, RDRF realizes a denser receptive field by taking more neighbor pixels along the spatial and temporal dimensions. Second, it features a self-supervised recurrent video denoising framework, which concurrently integrates distant and near-neighbor temporal features. This enables long-term bidirectional information aggregation, while mitigating error accumulation in the plain recurrent framework. Our method exhibits superior performance on both synthetic and real video denoising datasets. Codes will be available at <https://github.com/Wang-XiaoDingdd/RDRF>.

CCS CONCEPTS

• Computing methodologies → Reconstruction.

KEYWORDS

video denoising, self-supervision

*Both authors contributed equally to this research.

[†]Corresponding author.

Permission to make digital or hard copies of all or part of this work for personal or classroom use is granted without fee provided that copies are not made or distributed for profit or commercial advantage and that copies bear this notice and the full citation on the first page. Copyrights for components of this work owned by others than the author(s) must be honored. Abstracting with credit is permitted. To copy otherwise, or republish, to post on servers or to redistribute to lists, requires prior specific permission and/or a fee. Request permissions from permissions@acm.org.

MM '23, October 29–November 3, 2023, Ottawa, ON, Canada

© 2023 Copyright held by the owner/author(s). Publication rights licensed to ACM.

ACM ISBN 979-8-4007-0108-5/23/10...\$15.00

<https://doi.org/10.1145/3581783.3612228>

ACM Reference Format:

Zichun Wang, Yulun Zhang, Debing Zhang, and Ying Fu. 2023. Recurrent Self-Supervised Video Denoising with Denser Receptive Field. In *Proceedings of the 31st ACM International Conference on Multimedia (MM '23)*, October 29–November 3, 2023, Ottawa, ON, Canada. ACM, New York, NY, USA, 10 pages. <https://doi.org/10.1145/3581783.3612228>

1 INTRODUCTION

Video denoising is a fundamental topic in low-level computer vision tasks [14, 33, 42, 46, 47, 58]. Specifically, noise can greatly degrade the visual quality of videos, especially under light-deficient conditions. Besides, the poor visual quality of noisy videos will also adversely impact downstream computer vision tasks [12, 45].

Recently, thanks to powerful deep neural networks, supervised video denoising [15, 26, 32, 46–48] have achieved impressive performance. Regrettably, the success of supervised video denoising methods often relies on large-scale paired noisy-clean datasets. Nonetheless, collecting high-quality paired videos covering various types of sensors and noise levels can be extremely labor-intensive. Furthermore, paired videos are almost unavailable in some complex scenarios, e.g., microscopy videos and dynamic scene videos. Unlike image denoising datasets [1, 40], where clean images are collected based on either the long exposure time or averaging multiple noisy images, collecting videos can result in motion blur in dynamic scenes, which severely degrades their quality. Consequently, existing paired video denoising datasets are often captured under degraded or simplified settings [8, 15, 60], whose generalization ability to real world situations can be greatly constrained [15].

Therefore, to eliminate the dependence on large-scale paired datasets, several attempts have been made for self-supervised video denoising. Inspired by either the pioneer work Noise2Noise [25] or the subsequent blind spot networks [1, 2, 21, 22], previous studies can be divided into two categories, i.e., frame-based [1, 2, 13, 21] and concatenation-based [44] methods. However, their performance is limited by the insufficient receptive field on either the reference frame or the neighbor frames, as shown in Figure 1.

First, frame-based methods attempt to apply Noise2Noise [25] framework on videos. These methods align the consecutive frames using the estimated optical flow. Then, under the assumption that the warped frames are well-aligned, it adopts the Noise2Noise [25] strategy for self-supervised denoising. However, they are susceptible to the error resulting from inaccurate optical flow estimation, where the basic assumption, i.e., the same underlying clean signal, is no longer satisfied. Moreover, frame-based methods require reference frames to be masked to avoid learning identity mapping. This

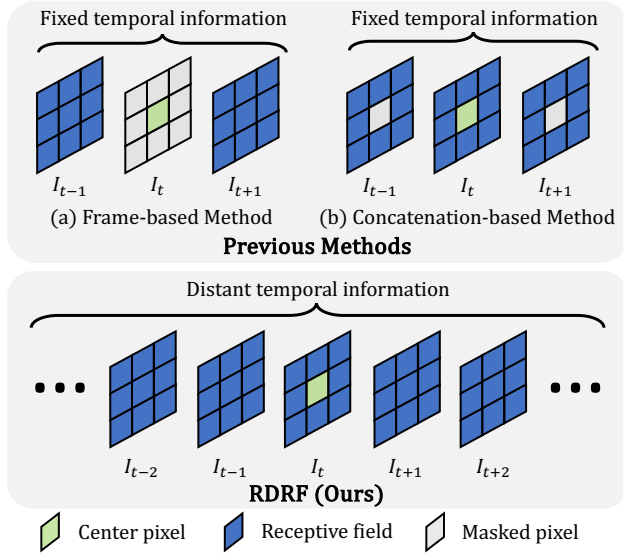


Figure 1: Receptive field comparison. (a) **Frame-based methods** [13, 27, 59] use neighbor frames only to predict the reference frame, and the reference frame is fully masked. (b) **Concatenation-based method** [44] treats the reference and neighbor frames in the same way, where the restricted receptive field for neighbors leads to under-utilization of temporal information. (c) **RDRF** realizes a denser receptive field of both reference and neighbor information. Besides, it adopts the recurrent framework under the blind spot requirement, which takes advantage of distant temporal information.

dramatically reduces the receptive field of these methods, where the useful information in the reference frame is greatly lost while restoring the reference frame itself. Second, inspired by the image blind spot networks [1, 2, 21], another line of work focuses on designing video blind spot networks. Recently, UDVD [44] extends the image blind-spot network [22] based on a video denoising network [47]. However, UDVD [44] applies the same blind spot processing to both the reference frame and neighboring frames, while this leads to a significant loss of neighbor frame information.

Apart from the limited receptive field, another challenge for existing methods is to fully utilize the temporal information. While long-range temporal features have been proven to be crucial for video restoration [5, 6, 16], current short-term temporal aggregation is insufficient, particularly for long-sequence videos. This limits the availability of long-term temporal information, as it only considers local neighbor frames within a very limited window size, which typically spans three or five contiguous frames [13, 44]. And simply enlarging the window size can bring challenges to the balance of efficiency and effectiveness. However, it cannot be solved by naively adopting existing recurrent fashion, since it breaks the blind spot requirement and thus fails to recover the clean scenes.

In this paper, we propose RDRF, a self-supervised video denoising method to tackle these issues. First, under a fine consideration of the blind spot requirement for self-supervision, RDRF realizes a denser receptive field. This allows for fully exploiting the information that is existed both in the reference frame and neighbor frames, providing valuable information for improved detail reconstruction.

Second, under the blind spot constraint, RDRF adopts the recurrent fashion. It significantly increases the usable temporal information, leveraging more inter-frame similarity to enhance the restoration process. Specifically, our method contains two parallel branches, focusing on the fusion of distant and near-neighbor temporal information respectively. For the long-range branch, we propose a Distant Feature Fusion module, which combines the reference blind spot feature with the temporally propagated non-blind feature in a spatially-adaptive way. For the local branch, we propose a Local Feature Extraction module, which utilizes 3D blind spot convolution to fully utilize the spatial and temporal local information, and also eases the error accumulation in the plain recurrent framework. By our design, the recovery can be aided by both distant and near neighbor frames with comprehensive exploitation.

We sum up our contributions in the following:

- We present a novel method for self-supervised video denoising, which fully exploits both reference and neighbor frames under blind spot requirement, enabling a denser receptive field for comprehensive information utilization.
- Towards full exploitation of temporal features, our method recurrently integrates distant and near-neighbor temporal features, which realizes robust long-term information aggregation and error accumulation mitigation concurrently.
- Experiments results show that our method achieves state-of-the-art performance on various synthetic and real world video denoising datasets.

2 RELATED WORK

In this section, we review relevant studies on supervised video denoising, unsupervised image and video denoising.

2.1 Supervised Video Denoising

Natural videos exhibit significant redundancy along the temporal dimension, which requires video denoising methods to fully utilize the temporal information compared to processing a single image only. Traditional methods group spatially and temporally similar patches [4, 31], but the searching process can be time-consuming, and the performance is sometimes unsatisfactory. Recently, deep learning based methods have shown better performance by employing a sliding window scheme to aggregate temporal information. ViDeNN [10] uses two CNN-based fusion networks, one for processing spatial and the other for temporal information. In order to better utilize temporal information to assist in the recovery of the current frame, some studies have introduced various components to advance the fusion process, e.g., optical flow [46, 58], deformable convolution [60], cascaded U-Net [47], non-local patch grouping [48], kernel prediction network [34, 54, 57] and channel shifting [43]. However, these methods may discard the distant temporal information, where only one or two frames before and after the reference frame are considered. Recently, the recurrent video denoising framework has attracted increasing attention owing to its capability to capture long-term temporal information. These methods typically rely on the bidirectional or unidirectional temporal feature, featuring guided deformable attention [7, 29], mimicked backward recurrent module [26], and low computational costs [32, 37, 55]. All of these methods are designed for supervised denoising, and cannot work when only noisy observations are provided.

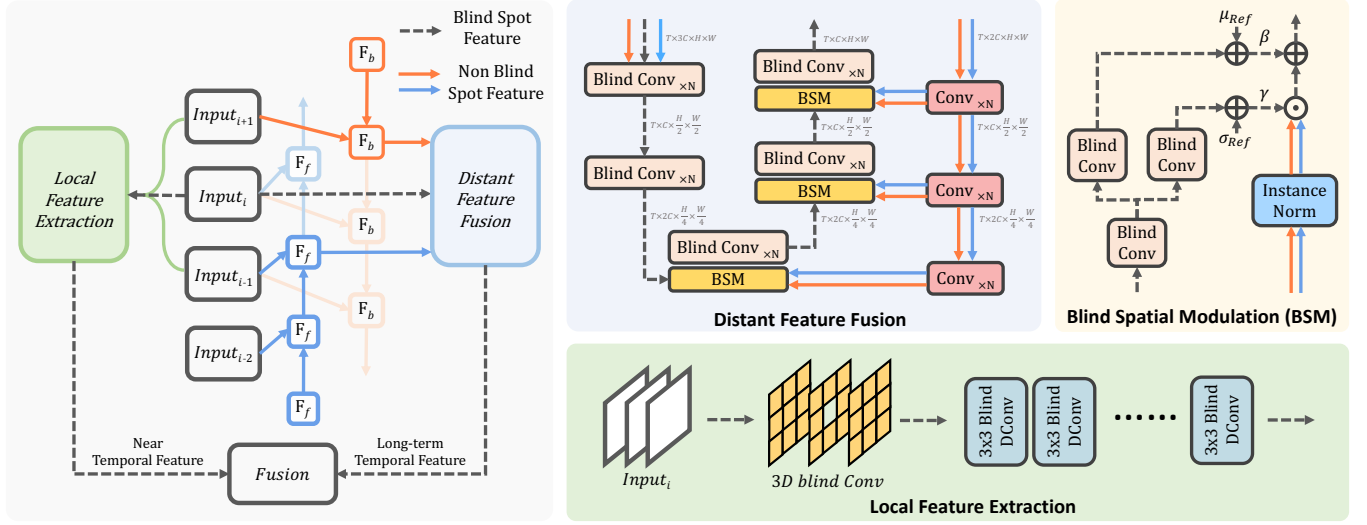


Figure 2: Illustration of the general structure of RDRF. Our approach comprises two branches, each with the specific goal, e.g., local textures and long-term information. Finally, the outputs from both branches are combined to produce the final result.

2.2 Unsupervised Image Denoising

Under situations where paired noisy-clean images are unavailable, researchers seek to exploit the internal information in noisy images. These methods are trained on different types of data, including pseudo noisy-clean pairs, noisy-noisy pairs, and noisy data only. For methods aiming to generate pseudo-noisy-clean pairs, GCBF [9] synthesizes realistic noisy images by a generative adversarial network (GAN), which is then advanced by introducing extra knowledge of a self-supervised network [53], or taking more noise components into account [19]. Besides, inspired by the semi-supervised method Noise2Noise [25], some methods are trained on noisy-noisy pairs. To synthesize noisy image pairs, several techniques have been proposed, e.g., sub-sampling from original images [18], generating noisier-noisy pairs [35, 56], or by a data augmentation technique [38]. Some other methods are trained directly on noisy images. Noise2Void [21] and Noise2Self [2] initially propose the blind spot network (BSN), while the performance and efficiency are unsatisfying. To this end, Laine19 [22], D-BSN [53] and Blind2Unblind [52] are further proposed with advanced BSN designs and better performance. Recently, the application of BSN is extended from spatially independent noise to spatially dependent real noise [24, 36, 51]. However, these methods still focus on denoising a single image, and the temporal information can not be utilized.

2.3 Unsupervised Video Denoising

Based on the method used, current self-supervised video denoising methods can be divided into two main categories: those based on Noise2Noise (N2N) [25] or the blind spot networks [2, 21, 22]. The first type of method follows the assumption of N2N, which requires noisy observations under the same scene. For videos, adjacent frames can be seen as under the same scene with motion transformation. Thus, under this assumption, Frame2Frame (F2F) [14] first warps adjacent frames based on the TV-L1 optical flow [61], then follows N2N for denoising. This is further enhanced with a trainable optical flow estimator [59] for more accurate alignment.

Nonetheless, the adopted image-based denoiser is not suitable for video denoising task. Therefore, Multi-Frame2Frame [13] takes multiple neighbor frames as input to predict the masked reference frame. A twin sampler strategy is also proposed to prevent from learning the identity mapping [27]. However, they all suffer from inaccurate motion and occlusion estimation, especially when the motion is relatively high or intensity conversion are not attributed to the translation. Moreover, they satisfy the self-supervision requirement at the cost of discarding the reference frame. The limited useful information significantly constrains their performance.

Another type of method try to extend the image blind spot network to videos, where the reference frame information can thus be utilized. Specifically, based on the architecture of FastDVDnet [47], UDVD [44] takes the stack of frames into a blind spot network, while the supporting neighbor features are processed under a constrained receptive field, resulting in destroyed temporal similar patterns due to their coarse consideration of the self-supervision requirement for videos. Also, current methods with short-term temporal aggregation fall short of valuable distant temporal information. This limits the availability of long-term similar patterns, as it only considers frames within limited window size, which typically operates on only three or five contiguous frames.

3 METHOD

In this section, we first go into details about the motivation, and then present detailed demonstrations of our two core designs, i.e., Distant Feature Fusion and Local Feature Extraction.

3.1 Motivation and Modeling

Despite the promising performance achieved by image denoising methods, video denoising intrinsically differs due to the huge amount of extra information along the temporal dimension [15, 46, 47, 58]. The recovery of a video frame requires two types of information: the reference frame provides one perfectly aligned noisy observation of the underlying scene, while its misaligned neighbor

frames offer abundant similar patterns for recovery. Therefore, designing a video denoising method necessitates the full exploitation of both the reference and neighbor frames.

Full exploitation for reference and neighbor frames. However, for self-supervised denoising, it is not feasible to simply increase the density of receptive fields and utilize all information, which violates the blind spot constraint [2, 21, 22] and leads to learning identity mapping. Therefore, the key lies in the careful consideration to maximize the receptive field, while respecting the blind spot requirement. Nonetheless, the coarse consideration of such constraint inevitably brings information loss and degraded performance for current methods. Some methods solely rely on the information from neighbor frames [13, 14, 14, 27, 44, 59], and the missing of the whole reference frame means the lack of a perfectly aligned noisy observation from the reference frame, leading to inferior performance. Other methods suffer from the destruction of useful hints in neighbor frames [44], since the reference and neighbor frames are processed in the same way following the blind spot requirement. The restricted receptive field originates from the under-consideration of the blind spot requirement. Instead, our observation is that, the blind spot for the reference frame is already enough for self-supervision. Instead, neighbor frames are not limited by such constraints, which it is usually omitted by previous studies, including the previous SOTA method UDVD [44].

Gathering long-term temporal information. Another challenge for previous methods is to effectively aggregate temporal information, especially for long-sequence videos. First, just as the spatial non-local similarity has been proven indispensable for image restoration [3, 28], leveraging more long-term dependencies along the temporal dimension is also the key to video denoising [15, 31, 48]. Unfortunately, previous methods are unable to accumulate distant temporal similarities, while using a large window size brings challenges for efficiency. Second, for distant temporal information aggregation, simply adopting a recurrent framework is also not an optimal choice. Recent studies have revealed error accumulation is inevitable due to the propagation mechanism [17, 20, 63], and relying on temporally propagated features only is not enough for effective exploitation of the redundant neighbor patterns.

Our method. We aim to address both of these issues in this paper. First, based on different blind spot requirements for reference and neighbor frames, we treat them in a blind and non-blind manner respectively. Second, toward full utilization of distant temporal information, at the same time easing error accumulation, we integrate both long-term and near-neighbor features in a concurrent way.

Problem modeling. Given a noisy video sequence of size $x \in \mathbb{R}^{T \times H \times W \times C}$, where C , T , H and W are the channel, video length, height, and width respectively. In Figure 2, we provide the architecture of RDRF, which contains two branches in parallel. For long-term temporal information aggregation, neighbor temporal features are first propagated forward and backward respectively without the blind spot requirement, which prevents the loss of temporal similar patterns in neighbor frames. The propagated long-term temporal features are then fused with the blind feature of the reference frame by the Distant Feature Fusion. For the near-temporal feature, Local Feature Extraction extracts the detailed structure within the temporally adjacent frames. Finally, the output of these two parallel branches is fused together as the final output.

3.2 Distant Feature Fusion

To address the severely limited receptive field and the insufficient long-term temporal features, we redesign the main components for self-supervised video denoising: propagation and fusion.

Temporal information propagation. Propagation decides the way we leverage the information that existed in a video sequence. Previous methods adopt local propagation [13, 14, 44], where the restoration can only be aided by the short-term temporal information. Instead, we take advantage of the bidirectional propagation scheme, where temporal information can be propagated both forward and backward for long-term temporal patterns. However, current supervised recurrent frameworks [5, 6] for I_i^{Clean} require I_i^{Noisy} as input, which breaks the requirement for self-supervision. A naive solution is to process neighbor frames 'blindly', in the same way as the current frame [44], while it results in the texture destruction in neighbor frame features. Instead, as shown in Figure 2, we first propagate the long-term information in a non-blind manner, where neighbor features can be fully extracted. Then, for a noisy input x_i , its neighboring frames x_{i-1} and x_{i+1} , the forward and backward propagated features denoted as h_{i-1}^f and h_{i+1}^b , the temporal propagation is computed as:

$$\begin{aligned} h_i^b &= F_b(x_{i+1}, h_{i+1}^b) \\ h_i^f &= F_f(x_{i-1}, h_{i-1}^f), \end{aligned} \quad (1)$$

where F_b and F_f denote the backward and forward propagation modules respectively. We implement F_b and F_f with Restormer [62] blocks for enhanced long-distance dependencies modeling. Here, note that the reference frame x_i itself will not be taken as the input of F_b and F_f for the blind spot requirement. In other words, only neighbor frames are processed in a "non-blind" manner, enabling long-term neighbor feature aggregation with a denser receptive field. By doing so, we are also free of the special structure of blind spot networks for F_b and F_f , allowing us to benefit from the latest design of the supervised method, e.g., Restormer block [62].

Fusion of reference and neighbor information. Next, after obtaining fully extracted temporal features from neighbor frames, the next step is to effectively fuse the information from the reference frame and the propagated features. Different from existing methods that directly concatenate reference and neighbor features, then process them through the blind spot network [44], we benefit from the non-blind neighbor features to better assist the recovery of the current frame in a spatially adaptive way, inspired by previous works [30, 39]. Specifically, our Distant Feature Fusion module takes two sets of features as inputs. A blind spot network [22] first takes the neighbor features and temporal propagated features, which employ four branches with limited receptive fields in distinct directions. To produce the blind spot, each branch applies a shift of a single pixel to the features. Following the implementation of this architecture, our Blind Spatial Modulation module remaps the distribution of temporal features to the reference frame. To generate the parameters β and γ , the reference feature is first concatenated with temporal features and fed into the blind convolutions following HQ-SSL [22]. Then we apply instance normalization on the temporal features as:

$$Net_i^c \leftarrow \frac{Net_i^c - \mu_i^c}{\sigma_i^c}, \quad (2)$$

where Nei_i^c is the concatenation of temporal propagated feature h_i^b from backward and h_i^f from forward at i^{th} frame in channel c . σ_i^c and μ_i^c is the standard deviation and mean for Nei_i^c as:

$$\begin{aligned}\mu_i^c &= \frac{1}{HW} \sum_{h,w} Nei_i^{c,h,w}, \\ \sigma_i^c &= \sqrt{\frac{1}{HW} \sum_{h,w} (Nei_i^{c,h,w} - \mu_i^c)^2}.\end{aligned}\quad (3)$$

where H and W are the height and width of Nei_i^c . Then, based on the reference frame statistic, we update β and γ as:

$$\begin{aligned}\beta &\leftarrow \beta + \hat{\mu}_i^c, \\ \gamma &\leftarrow \gamma + \hat{\sigma}_i^c,\end{aligned}\quad (4)$$

where $\hat{\mu}_i^c$ and $\hat{\sigma}_i^c$ denotes the mean and standard deviation of reference feature. Finally, we can remap the distribution for the non-blind temporal neighbor feature as follows:

$$F_{Ref} \leftarrow F_{Ref} \cdot \gamma + \beta. \quad (5)$$

The neighbor features are re-modulated in a spatially adaptive way, conditioned on the scene difference between the frames. This is then processed by the blind convolution for the overall output.

3.3 Local Feature Extraction

The recurrent network can naturally aggregate long-term temporal information, bringing abundant similar patterns from its distant neighbor frames. However, errors generated in each time step can be accumulated meanwhile [17, 20, 63], which limits the effectiveness of auxiliary neighbor features. Thus, relying on the propagated neighbor features is not enough for recovery.

In addition, the closer to the reference frame, the more similar the content of neighbor frames. These neighbor frames typically contain the most useful information, which should be carefully considered. Thus, besides capturing the temporally long-term information, we further propose the Local Feature Extraction module to better focus on the near neighbor feature.

Specifically, the main goal of blind spot networks is to ensure that the output at each position is not influenced by the input. Under such requirement, we fully utilize both spatially and temporally neighbor pixels to recover the center masked pixel. As shown in Figure 2, we propose a blind 3D convolution for near-neighbor spatial-temporal features extraction, which is defined as:

$$Out_i^c = [x_{i-1}, x_i, x_{i+1}] \otimes (Wei_i^c \circ Mask), \quad (6)$$

where Out_i^c is the output c^{th} feature of the 3D blind convolution, Wei_i^c and $Mask$ denote the $3 \times 3 \times 3$ kernel weight and corresponding binary mask m , \otimes and \circ denote convolution and element-wise product operator. Note that the center of the kernel weight is set to zero, in order to meet the self-supervised blind spot constraint. Then, inspired by the previous self-supervised image denoising method [53], we maintain the blind spot requirement by stacking dilated convolution with a stride of 2 to extract deep local features.

Finally, after obtaining the near-neighbor and distant temporal features, we use 1×1 convolutions to gradually transform the high-dimensional feature into the final output.

4 EXPERIMENTS

In this section, we introduce datasets and setup details, providing the performance comparison and corresponding analysis.

4.1 Dataset and Setup Details

Natural videos. We train our method with the widely used DAVIS train set [41] for the removal of synthetic Gaussian noise, and conduct experiments with natural videos by introducing independent and identically distributed Gaussian noise. We evaluate on two datasets, including Davis test set [41] and Set8 [47] dataset. Four videos from the Derfs Test Media collection [13] and four GoPro-shot footage make up the Set8 dataset. To maintain consistency with previous settings, we use initial 85 frames in the Derfs dataset.

Raw videos. The CRVD dataset [60] is a collection of real-world raw videos used for fine-tuning and testing. It includes 6 scenes for training and 5 scenes for evaluation and testing. Each scene contains 7 frames with 5 different noise levels. The ground truth frames are produced by taking the average of multiple noisy frames.

Implementation details. Following previous works [44], for natural video denoising, we adopt a batch size of 32 with \mathcal{L}_{log} between the noisy and output videos to combine the Gaussian prior [22, 44]. For raw video, we adopt a batch size of 8 with \mathcal{L}_2 loss. The length of the input sequence is 9 for natural videos and 7 for raw videos. To save training time for natural videos, we output and supervise the central frame and keep this setting while testing. The learning rate starts with $1e-4$, where the Adam optimizer is adopted. For raw dataset, overfitting can be severe since its size is extremely small. Though we get promising results with a simple way of fusion, *i.e.*, blind convolutions in Distant Feature Fusion, extra BSM does not yield satisfactory results, so we do not adopt BSM for raw dataset. We conduct experiments in PyTorch 1.8.0 and the Nvidia RTX 3090.

Metrics. Peak signal-to-noise ratio (PSNR) and structural similarity (SSIM) are the two metrics used for evaluation [50]. The larger value of these two metrics denotes better image quality. We compare the performance of RDRF with several traditional video denoising methods, *e.g.*, VNLB [23], VBM4D [31], supervised methods, *e.g.*, VNLnet [11], DVDnet [46], FastDVDnet [47], FloRNN [26], and unsupervised methods, *e.g.*, MF2F [13], UDVD [44].

4.2 Evaluation on Natural Videos

We conduct extensive experiments to compare our method with three types of methods, including traditional, supervised and unsupervised methods. The results on the Set8 dataset and the Davis test set are reported in Table 1 and Table 2 respectively.

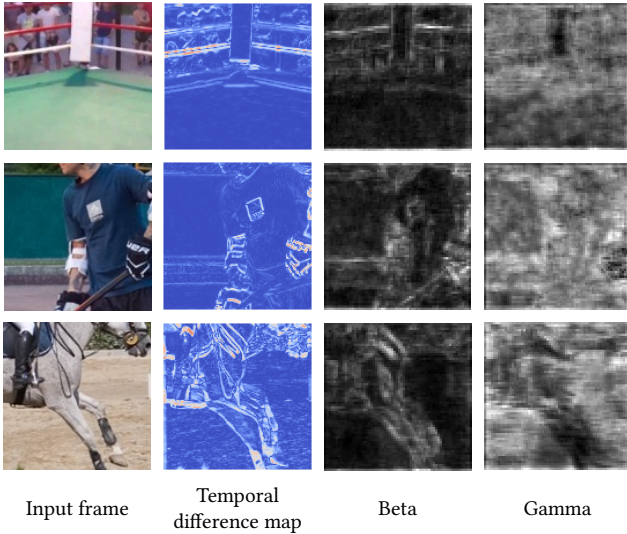
We obtain superior results in quantitative and qualitative metrics than previous unsupervised methods, where the qualitative results on Set8 and Davis benchmark datasets are shown in Figure 4 and Figure 5, respectively. Our results show more detailed structures, also smoother in the flat areas. For UDVD [44], since the temporal neighbor pixels are masked from the receptive field, the limited useful information brings inferior performance. For MF2F [44], the performance is limited by the lack of information in the reference frame and the error by misalignment. Instead, our method can fully exploit the spatial and temporal neighbors, also extracting the distant and near-temporal information. Thanks to these designs, our method outperforms previous unsupervised methods, which is even comparable to the supervised video denoising method.

Set8 sigma	Traditional		Supervised				Unsupervised		
	VBM4D [31]	VNLB [23]	VNLnet [11]	DVDnet [46]	FastDVDnet [47]	FloRNN [26]	MF2F [13]	UDVD [44]	RDRF (Ours)
10	36.05/-	37.26/-	37.28/.9606	36.08/.9510	36.44/.9540	<u>37.57/.9639</u>	36.01/.9379	36.36/.9510	36.67/.9547
20	32.19/-	33.72/-	34.02/.9273	33.49/.9182	33.43/.9196	<u>34.67/.9379</u>	33.79/.9115	33.53/.9167	34.00/.9251
30	30.00/-	31.74/-	-	31.68/.8862	31.68/.8889	<u>32.97/.9138</u>	32.20/.8831	31.88/.8865	32.39/.8978
40	28.48/-	30.39/-	30.72/.8622	30.46/.8564	30.46/.8608	<u>31.75/.8911</u>	30.64/.8413	30.72/.8595	31.23/.8725
50	27.33/-	29.24/-	-	29.53/.8289	29.53/.8351	<u>30.80/.8696</u>	28.90/.7775	29.81/.8349	30.31/.8490
avg	30.81/-	32.47/-	-	32.29/.8881	32.31/.8917	<u>33.55/.9153</u>	32.31/.8703	32.46/.8897	32.92/.8998

Table 1: Performance comparison on Set8 [47] dataset. The best results for un-/supervised methods are in bold and underlined.

Davis sigma	Traditional		Supervised				Unsupervised		
	VBM4D [31]	VNLB [23]	VNLnet [11]	DVDnet [46]	FastDVDnet [47]	FloRNN [26]	MF2F [13]	UDVD [44]	RDRF (Ours)
10	37.58/-	38.85/-	39.56/.9707	38.13/.9657	38.71/.9672	<u>40.16/.9755</u>	38.04/.9566	39.17/.9700	39.54/.9717
20	33.88/-	35.68/-	36.53/.9464	35.70/.9422	35.77/.9405	<u>37.52/.9564</u>	35.61/.9359	35.94/.9428	36.40/.9473
30	31.65/-	33.73/-	-	34.08/.9188	34.04/.9167	<u>35.89/.9440</u>	33.65/.9065	34.09/.9178	34.55/.9245
40	30.05/-	32.32/-	33.32/.8996	32.86/.8962	32.82/.8949	<u>34.66/.9286</u>	31.50/.8523	32.79/.8949	33.23/.9032
50	28.80/-	31.13/-	-	31.85/.8745	31.86/.8747	<u>33.67/.9131</u>	29.39/.7843	31.80/.8739	32.20/.8832
avg	32.39/-	34.34/-	-	34.52/.9195	34.64/.9188	<u>36.38/.9435</u>	33.64/.8871	34.76/.9199	35.18/.9260

Table 2: Performance comparison on Davis [41] dataset. The best results for un-/supervised methods are in bold and underlined.

Figure 3: Illustrations on the pixel-wise difference between two consecutive frames, and corresponding learned modulation parameters, i.e., γ and β .

4.3 Evaluation on Real Raw Data

We evaluate the performance on the real world raw video denoising dataset [60] in Table 3. Our method outperforms UDVD [44] on almost all the noise levels due to our better utilization of reference and neighbor features. Furthermore, under this setting, other frame-based methods like MF2F [13] cannot be directly applied to raw videos, since their method relies on a pre-trained backbone that only works in the RGB color domain. We also compare the performance of our RDRF with supervised methods RViDeNet [60]. We achieve better quantitative performance than UDVD and RViDeNet

at all noise levels. We emphasize that UDVD is directly trained on the mosaiced raw videos, and RViDeNet is pre-trained and fine-tuned on paired videos. In Figure 6, we provide visualizations of restored frames on the CRVD dataset. Our method can better reconstruct the fine textures by the full exploitation of the reference and neighbor frames, also with the temporal similar patterns.

4.4 Analysis of the Proposed Method

Visualization of Blind Spatial Modulation. The purpose of the Blind Spatial Modulation module is to fuse the current frame and its adjacent temporal features in a spatially adaptive way. We visualize the corresponding feature maps in Figure 3. Regions with smaller motion correspond to smaller beta and larger gamma values. This is because when the adjacent frame has a higher degree of similarity, it can be directly used for recovery without much modification (smaller beta), and also being indispensable in the recovery process (larger gamma). As a result, this allows for the effective utilization of temporal features, while implicitly capturing motion information.

Visualization on receptive field. To better validate the significance of a denser receptive field, we provide the corresponding visualization shown in Figure 7. As can be seen, when the scene motion is small, the center pixel of the neighbor frame is most similar to the center pixel of the reference frame. This proves that the center pixels of neighbor frames can provide the most useful hints to restoring the reference frame, while UDVD [53] is unable to leverage this information, due to its under-utilization of the neighbor features. Also, the local aggregation also limits the range of available temporal information. Our approach, on the other hand, can efficiently use both distant temporal information and the current frame. By focusing on the most similar patterns for the restoration, it enables the potential for better performance.

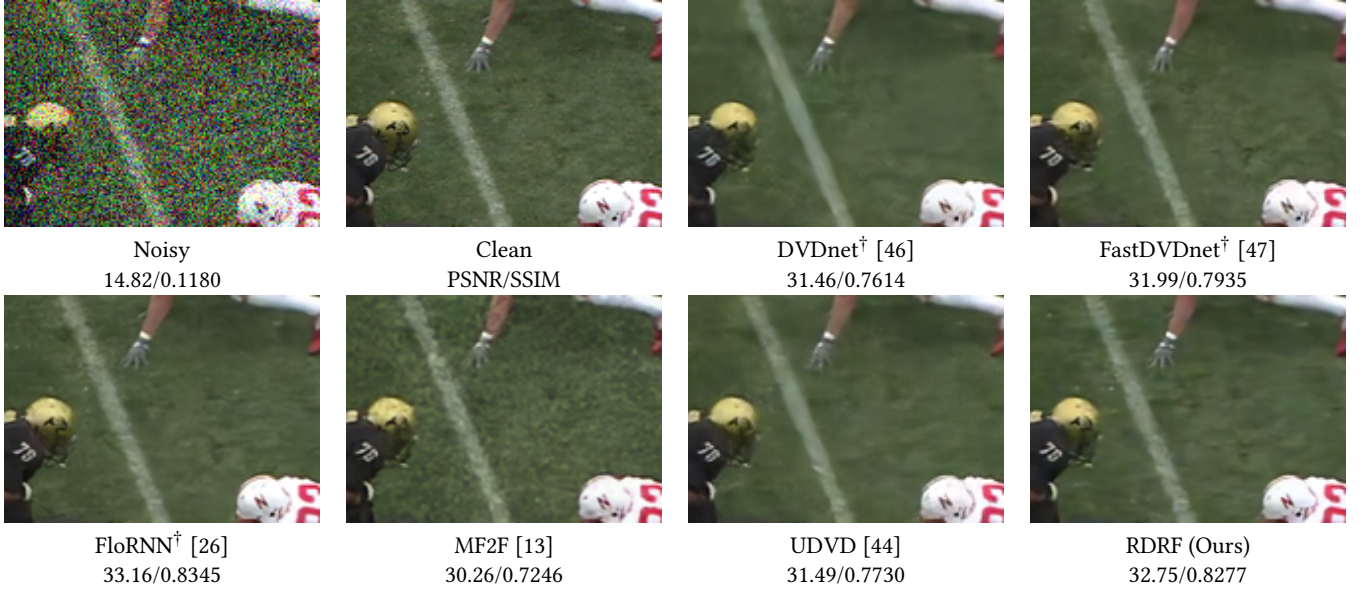


Figure 4: Visual quality comparison on Set8 dataset. Supervised methods are marked with [†].

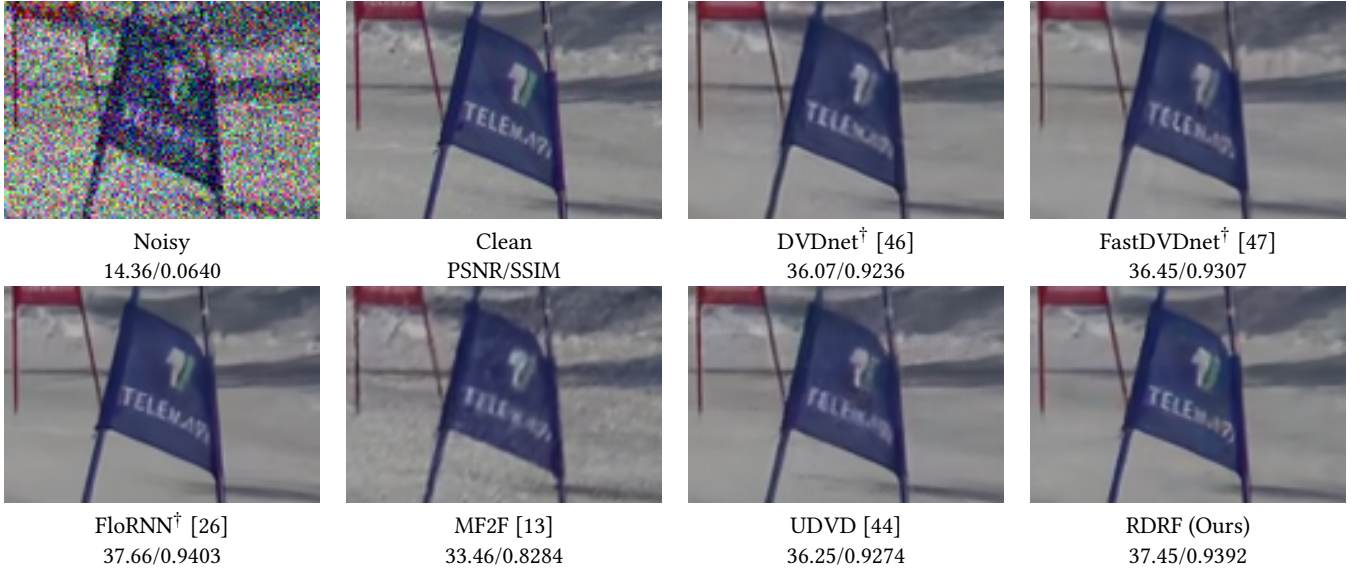


Figure 5: Visual quality comparison on Davis dataset. Supervised methods are marked with [†].

Ablation studies on the proposed modules. Our method consists of two branches for temporally long-range information aggregation and local neighbor information processing. For both the two parallel branches, our method can fully exploit the features of the reference frame and its temporal neighbors. We validate that both of these branches are indispensable for self-supervised video denoising. We do ablation studies on the Set8 dataset, as seen in Table 4.

Ours w/o Distant Feature Fusion. The lack of long-term features will cause a significant limitation on the scope of temporal information, where a large number of similarity patterns in the neighbor frames can not be utilized. This leads to a 1.41 dB drop in PSNR.

Ours w/ blind convolutions for propagation. To further validate that only gathering distant temporal features without the dense

receptive field for neighbor frames is not enough, we implement F_b and F_f with blind convolutions following HQ-SSL [22]. It can be found that full utilization of neighbor frames boost recovery performance, proving the importance of the denser receptive field. **Ours w/o Local Feature Extraction.** When relying solely on temporal propagation, the accumulated error during the propagation process will harm the performance of the network. The PSNR of the network decreases by 0.16 dB without Local Feature Extraction. **Ours w/o Blind Spatial Modulation.** Furthermore, the way to effectively fuse the reference and neighbor features is also the key to video restoration. Blind Spatial Modulation can explicitly consider the motion changes in the video and modulate the neighboring feature according to the motion in different regions. When we

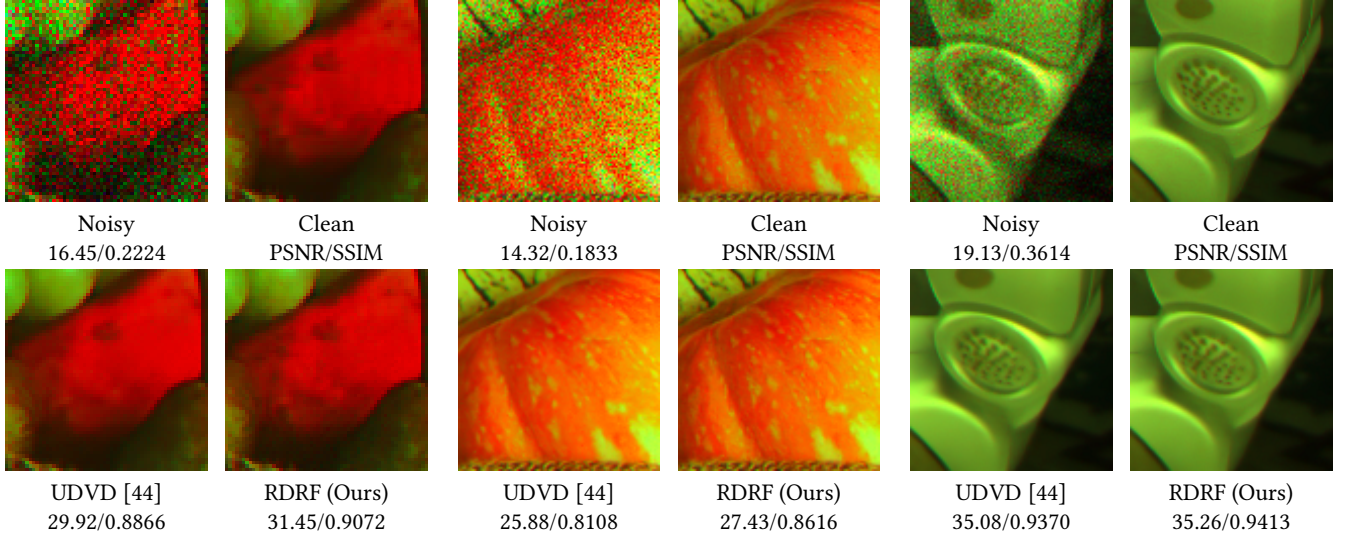


Figure 6: Visual quality comparison on CRVD dataset [60].

Method	Supervised					Unsupervised	
ISO	FastDVDnet [47]	RViDeNet [60]	EDVR [49]	LLRVD [15]	FloRNN [26]	UDVD [44]	RDRF (Ours)
1600	43.43/0.9866	47.74/0.9938	47.59/0.9932	47.91/0.9941	<u>48.81/0.9956</u>	48.02/0.9982	48.38/0.9983
3200	42.91/0.9844	45.91/0.9911	45.15/0.9889	46.02/0.9913	<u>47.05/0.9933</u>	46.44/0.9980	46.86/0.9981
6400	40.29/0.9793	43.85/0.9880	43.10/0.9848	44.13/0.9885	<u>45.09/0.9910</u>	44.74/0.9972	45.24/0.9975
12800	36.05/0.9613	41.20/0.9819	40.88/0.9779	41.58/0.9827	<u>42.63/0.9866</u>	42.21/0.9966	42.72/0.9969
25600	36.50/0.9400	41.17/0.9821	41.03/0.9785	41.53/0.9829	<u>42.19/0.9872</u>	42.13/0.9951	42.25/0.9948
avg	39.84/0.9703	43.97/0.9874	43.55/0.9847	44.23/0.9879	<u>45.15/0.9907</u>	44.71/0.9970	45.09/0.9971

Table 3: Performance comparison on CRVD [60] dataset. The best results for un-/supervised methods are in bold and underlined.

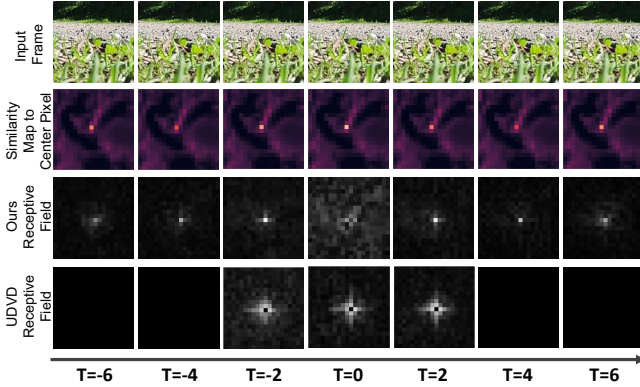


Figure 7: The degree of similarity to the center pixel of the reference frame (T=0) and the receptive field comparison. Our method can focus on the most similar positions, i.e., the center pixels of neighbor frames, with a long temporal range. While UDVD [44] is unable to utilize long-term information, and pixels most focused on by UDVD may not contain the most useful information without the dense receptive field.

remove the Blind Spatial Modulation, it makes the network unable to dynamically perform the fusion process, where a fixed fusion can lead to a decrease in performance.

Method	PSNR	SSIM
Ours w/o Distant Feature Fusion	31.32	0.8563
Ours w/ blind convolutions for propagation	32.21	0.8865
Ours w/o Local Feature Extraction	32.57	0.8933
Ours w/o Blind Spatial Modulation	32.52	0.8925
Ours full	32.73	0.8965

Table 4: Ablation studies on the proposed method.

5 CONCLUSION

In this paper, we present RDRF to tackle the challenges of self-supervised video denoising, including insufficient utilization of reference and neighbor information, also the limited available temporal feature. Our method consists of two branches for temporal long-range information aggregation and local neighbor information extraction. This enables our method fully exploit the information of spatial and temporal neighbors. Extensive results on both synthetic and real videos validate our superiority.

Acknowledgement This work was supported by the National Natural Science Foundation of China (62171038, 62171042, and 62088101), the R&D Program of Beijing Municipal Education Commission (KZ202211417048), and the Fundamental Research Funds for the Central Universities.

REFERENCES

- [1] Abdelrahman Abdelhamed, Stephen Lin, and Michael S Brown. 2018. A high-quality denoising dataset for smartphone cameras. In *CVPR*. 1692–1700.
- [2] Joshua Batson and Loic Royer. 2019. Noise2self: Blind denoising by self-supervision. In *ICML*. 524–533.
- [3] Antoni Buades, Bartomeu Coll, and J-M Morel. 2005. A non-local algorithm for image denoising. In *CVPR*. 60–65.
- [4] Antoni Buades, Jose-Luis Lisani, and Marko Miladinović. 2016. Patch-based video denoising with optical flow estimation. *IEEE TIP* 25, 6 (2016), 2573–2586.
- [5] Kelvin CK Chan, Xintao Wang, Ke Yu, Chao Dong, and Chen Change Loy. 2021. Basicvnr: The search for essential components in video super-resolution and beyond. In *CVPR*. 4947–4956.
- [6] Kelvin CK Chan, Shangchen Zhou, Xiangyu Xu, and Chen Change Loy. 2022. BasicVSR++: Improving video super-resolution with enhanced propagation and alignment. In *CVPR*. 5972–5981.
- [7] Kelvin CK Chan, Shangchen Zhou, Xiangyu Xu, and Chen Change Loy. 2022. On the generalization of basicvnr++ to video deblurring and denoising. *arXiv preprint arXiv:2204.05308* (2022).
- [8] Chen Chen, Qifeng Chen, Minh N Do, and Vladlen Koltun. 2019. Seeing motion in the dark. In *ICCV*. 3185–3194.
- [9] Jingwen Chen, Jiawei Chen, Hongyang Chao, and Ming Yang. 2018. Image blind denoising with generative adversarial network based noise modeling. In *CVPR*. 3155–3164.
- [10] Michele Claus and Jan Van Gemert. 2019. Videnn: Deep blind video denoising. In *CVPR Workshops*. 0–0.
- [11] Axel Davy, Thibaud Ehret, Jean-Michel Morel, Pablo Arias, and Gabriele Facciolo. 2019. A non-local CNN for video denoising. In *ICIP*. 2409–2413.
- [12] Xueqing Deng, Peng Wang, Xiaochen Lian, and Shawn Newsam. 2022. NightLab: A dual-level architecture with hardness detection for segmentation at night. In *CVPR*. 16938–16948.
- [13] Valéry Dewil, Jérémy Anger, Axel Davy, Thibaud Ehret, Gabriele Facciolo, and Pablo Arias. 2021. Self-supervised training for blind multi-frame video denoising. In *WACV*. 2724–2734.
- [14] Thibaud Ehret, Axel Davy, Jean-Michel Morel, Gabriele Facciolo, and Pablo Arias. 2019. Model-blind video denoising via frame-to-frame training. In *CVPR*. 11369–11378.
- [15] Ying Fu, Zichun Wang, Tao Zhang, and Jun Zhang. 2022. Low-light Raw Video Denoising with a High-quality Realistic Motion Dataset. *IEEE TMM (Early Access)* (2022).
- [16] Muhammad Haris, Gregory Shakhnarovich, and Norimichi Ukita. 2019. Recurrent back-projection network for video super-resolution. In *CVPR*. 3897–3906.
- [17] Cong Huang, Jiahao Li, Bin Li, Dong Liu, and Yan Lu. 2022. Neural compression-based feature learning for video restoration. In *CVPR*. 5872–5881.
- [18] Tao Huang, Songjiang Li, Xu Jia, Huchuan Lu, and Jianzhuang Liu. 2021. Neighbor2neighbor: Self-supervised denoising from single noisy images. In *CVPR*. 14781–14790.
- [19] Geonwoon Jang, Wooseok Lee, Sanghyun Son, and Kyoung Mu Lee. 2021. C2n: Practical generative noise modeling for real-world denoising. In *ICCV*. 2350–2359.
- [20] Jaeyeon Kang, Seoung Wug Oh, and Seon Joo Kim. 2022. Error compensation framework for flow-guided video inpainting. In *ECCV*. 375–390.
- [21] Alexander Krull, Tim-Oliver Buchholz, and Florian Jug. 2019. Noise2void-learning denoising from single noisy images. In *CVPR*. 2129–2137.
- [22] Samuli Laine, Tero Karras, Jaakko Lehtinen, and Timo Aila. 2019. High-quality self-supervised deep image denoising. In *NIPS*. 6970–6980.
- [23] Marc Lebrun, Antoni Buades, and Jean-Michel Morel. 2013. A nonlocal Bayesian image denoising algorithm. *SIAM Journal on Imaging Sciences* 6, 3 (2013), 1665–1688.
- [24] Wooseok Lee, Sanghyun Son, and Kyoung Mu Lee. 2022. AP-BSN: Self-Supervised Denoising for Real-World Images via Asymmetric PD and Blind-Spot Network. In *CVPR*. 17725–17734.
- [25] Jaakko Lehtinen, Jacob Munkberg, Jon Hasselgren, Samuli Laine, Tero Karras, Miika Aittala, and Timo Aila. 2018. Noise2Noise: Learning Image Restoration without Clean Data. In *ICML*. 2965–2974.
- [26] Junyi Li, Xiaohe Wu, Zhenxing Niu, and Wangmeng Zuo. 2022. Unidirectional Video Denoising by Mimicking Backward Recurrent Modules with Look-Ahead Forward Ones. In *ECCV*. 592–609.
- [27] Yanghao Li, Bichuan Guo, Jiangtao Wen, Zhen Xia, Shan Liu, and Yuxing Han. 2021. Learning model-blind temporal denoisers without ground truths. In *ICASSP*. 2055–2059.
- [28] Jingyun Liang, Jiezhang Cao, Guolei Sun, Kai Zhang, Luc Van Gool, and Radu Timofte. 2021. Swinir: Image restoration using swin transformer. In *ICCV*. 1833–1844.
- [29] Jingyun Liang, Yuchen Fan, Xiaoyu Xiang, Rakesh Ranjan, Eddy Ilg, Simon Green, Jiezhang Cao, Kai Zhang, Radu Timofte, and Luc V Gool. 2022. Recurrent video restoration transformer with guided deformable attention. *NIPS* (2022), 378–393.
- [30] Liying Lu, Wenbo Li, Xin Tao, Jiangbo Lu, and Jiaya Jia. 2021. Masa-sr: Matching acceleration and spatial adaptation for reference-based image super-resolution. In *CVPR*. 6368–6377.
- [31] Matteo Maggioni, Giacomo Boracchi, Alessandro Foi, and Karen Egiazarian. 2012. Video denoising, deblurring, and enhancement through separable 4-D nonlocal spatiotemporal transforms. *IEEE TIP* 21, 9 (2012), 3952–3966.
- [32] Matteo Maggioni, Yibin Huang, Cheng Li, Shuai Xiao, Zhongqian Fu, and Fenglong Song. 2021. Efficient multi-stage video denoising with recurrent spatio-temporal fusion. In *CVPR*. 3466–3475.
- [33] Sachin Mehta, Amit Kumar, Fitsum Reda, Varun Nasery, Vikram Mulukutla, Rakesh Ranjan, and Vikas Chandra. 2021. Evnrnet: Efficient video restoration on edge devices. In *ACM MM*. 983–992.
- [34] Ben Mildenhall, Jonathan T Barron, Jiawen Chen, Dillon Sharlet, Ren Ng, and Robert Carroll. 2018. Burst denoising with kernel prediction networks. In *CVPR*. 2502–2510.
- [35] Nick Moran, Dan Schmidt, Yu Zhong, and Patrick Coady. 2020. Noisier2noise: Learning to denoise from unpaired noisy data. In *CVPR*. 12064–12072.
- [36] Reyhaneh Neshatavar, Mohsen Yavartanoo, Sanghyun Son, and Kyoung Mu Lee. 2022. CVF-SID: Cyclic multi-Variate Function for Self-Supervised Image Denoising by Disentangling Noise from Image. In *CVPR*. 17583–17591.
- [37] Piotr Kopa Ostrowski, Efklidis Katsaros, Daniel Węsierski, and Anna Jezierska. 2022. BP-EVD: Forward Block-Output Propagation for Efficient Video Denoising. *IEEE TIP* 31 (2022), 3809–3824.
- [38] Tongyao Pang, Huan Zheng, Yuhui Quan, and Hui Ji. 2021. Recorrputed-to-recorrputed: unsupervised deep learning for image denoising. In *CVPR*. 2043–2052.
- [39] Taesung Park, Ming-Yu Liu, Ting-Chun Wang, and Jun-Yan Zhu. 2019. Semantic image synthesis with spatially-adaptive normalization. In *CVPR*. 2337–2346.
- [40] Tobias Plotz and Stefan Roth. 2017. Benchmarking denoising algorithms with real photographs. In *CVPR*. 1586–1595.
- [41] Jordi Pont-Tuset, Federico Perazzi, Sergi Caelles, Pablo Arbeláez, Alex Sorkine-Hornung, and Luc Van Gool. 2017. The 2017 davis challenge on video object segmentation. (2017).
- [42] Chenyang Qi, Junming Chen, Xin Yang, and Qifeng Chen. 2022. Real-time Streaming Video Denoising with Bidirectional Buffers. In *ACM MM*. 2758–2766.
- [43] Xuejian Rong, Denis Demandolx, Kevin Matzen, Priyam Chatterjee, and Yingli Tian. 2020. Burst denoising via temporally shifted wavelet transforms. In *ECCV*. 240–256.
- [44] Dev Yashpal Sheth, Sreyas Mohan, Joshua L Vincent, Ramon Manzanor, Peter A Crozier, Mitesh M Khapra, Eero P Simoncelli, and Carlos Fernandez-Granda. 2021. Unsupervised deep video denoising. In *ICCV*. 1759–1768.
- [45] Karasawa Takumi, Kohei Watanabe, Qishen Ha, Antonio Tejero-De-Pablos, Yoshitaka Ushiku, and Tatsuya Harada. 2017. Multispectral Object Detection for Autonomous Vehicles. In *ACM MM Workshops*. 35–43.
- [46] Matias Tassano, Julie Delon, and Thomas Veit. 2019. Dvdnet: A fast network for deep video denoising. In *ICIP*. 1805–1809.
- [47] Matias Tassano, Julie Delon, and Thomas Veit. 2020. Fastdvdnet: Towards real-time deep video denoising without flow estimation. In *CVPR*. 1354–1363.
- [48] Gregory Vaksman, Michael Elad, and Peyman Milanfar. 2021. Patch craft: Video denoising by deep modeling and patch matching. In *ICCV*. 2157–2166.
- [49] Xintao Wang, Kelvin CK Chan, Ke Yu, Chao Dong, and Chen Change Loy. 2019. Edvr: Video restoration with enhanced deformable convolutional networks. In *CVPR Workshops*. 0–0.
- [50] Zhou Wang, Alan C Bovik, Hamid R Sheikh, and Eero P Simoncelli. 2004. Image quality assessment: from error visibility to structural similarity. *IEEE TIP* 13, 4 (2004), 600–612.
- [51] Zichun Wang, Ying Fu, Ji Liu, and Yulun Zhang. 2023. LG-BPN: Local and Global Blind-Patch Network for Self-Supervised Real-World Denoising. In *CVPR*. 18156–18165.
- [52] Zejin Wang, Jiazhang Liu, Guoqing Li, and Hua Han. 2022. Blind2Unblind: Self-Supervised Image Denoising with Visible Blind Spots. In *CVPR*. 2027–2036.
- [53] Xiaohe Wu, Ming Liu, Yue Cao, Dongwei Ren, and Wangmeng Zuo. 2020. Unpaired learning of deep image denoising. In *ECCV*. 352–368.
- [54] Zhihao Xia, Federico Perazzi, Michael Gharbi, Kalyan Sunkavalli, and Ayan Chakrabarti. 2020. Basis prediction networks for effective burst denoising with large kernels. In *CVPR*. 11844–11853.
- [55] Liuyu Xiang, Jundong Zhou, Jirui Liu, Zerun Wang, Haidong Huang, Jie Hu, Jungong Han, Yuchen Guo, and Guiguang Ding. 2022. ReMoNet: Recurrent Multi-Output Network for Efficient Video Denoising. In *AAAI*. 2786–2794.
- [56] Jun Xu, Yuan Huang, Ming-Ming Cheng, Li Liu, Fan Zhu, Zhou Xu, and Ling Shao. 2020. Noisy-as-clean: Learning self-supervised denoising from corrupted image. *IEEE TIP* 29 (2020), 9316–9329.
- [57] Xiangyu Xu, Muchen Li, Wenxiu Sun, and Ming-Hsuan Yang. 2020. Learning spatial and spatio-temporal pixel aggregations for image and video denoising. *IEEE TIP* 29 (2020), 7153–7165.
- [58] Tianfan Xue, Baian Chen, Jiajun Wu, Donglai Wei, and William T Freeman. 2019. Video enhancement with task-oriented flow. *IJCV* 127 (2019), 1106–1125.
- [59] Songhyun Yu, Bumjun Park, Junwoo Park, and Jechang Jeong. 2020. Joint learning of blind video denoising and optical flow estimation. In *CVPR Workshops*. 500–501.

- [60] Huanjing Yue, Cong Cao, Lei Liao, Ronghe Chu, and Jingyu Yang. 2020. Supervised raw video denoising with a benchmark dataset on dynamic scenes. In *CVPR*. 2301–2310.
- [61] Christopher Zach, Thomas Pock, and Horst Bischof. 2007. A duality based approach for realtime tv-l 1 optical flow. In *Joint Pattern Recognition Symposium*. 214–223.
- [62] Syed Waqas Zamir, Aditya Arora, Salman Khan, Munawar Hayat, Fahad Shahbaz Khan, and Ming-Hsuan Yang. 2022. Restormer: Efficient transformer for high-resolution image restoration. In *CVPR*. 5728–5739.
- [63] Kun Zhou, Wenbo Li, Liying Lu, Xiaoguang Han, and Jiangbo Lu. 2022. Revisiting temporal alignment for video restoration. In *CVPR*. 6053–6062.